

Domain Architecture of the DRpp29 Protein and Its Interaction with the RNA Subunit of *Dictyostelium discoideum* RNase P

Vassiliki Stamatopoulou,[‡] Chrisavgi Toumpeki,[‡] Andreas Tzakos,[§] Anastassios Vourekas,^{*,‡,||} and Denis Drainas^{*,‡}

[‡]Department of Biochemistry, School of Medicine, University of Patras, 26500 Patras, Greece, and [§]Department of Chemistry, Section of Organic Chemistry and Biochemistry, University of Ioannina, 45110 Ioannina, Greece. ^{||}Present address: Department of Pathology and Laboratory Medicine, Division of Neuropathology, University of Pennsylvania School of Medicine, Philadelphia, PA 19104.

Received August 13, 2010; Revised Manuscript Received November 16, 2010

ABSTRACT: *Dictyostelium discoideum* nuclear RNase P is a ribonucleoprotein complex that displays similarities with its counterparts from higher eukaryotes such as the human enzyme, but at the same time it retains distinctive characteristics. In the present study, we report the molecular cloning and interaction details of DRpp29 and RNase P RNA, two subunits of the RNase P holoenzyme from *D. discoideum*. Electrophoretic mobility shift assays exhibited that DRpp29 binds specifically to the RNase P RNA subunit, a feature that was further confirmed by the molecular modeling of the DRpp29 structure. Moreover, deletion mutants of DRpp29 were constructed in order to investigate the domains of DRpp29 that contribute to and/or are responsible for the direct interaction with the *D. discoideum* RNase P RNA. A eukaryotic specific, lysine- and arginine-rich region was revealed, which seems to facilitate the interaction between these two subunits. Furthermore, we tested the ability of wild-type and mutant DRpp29 to form active RNase P enzymatic particles with the *Escherichia coli* RNase P RNA.

Ribonuclease P (RNase P) is a universally conserved enzyme that is involved in the maturation of the precursor tRNAs by the removal of their 5' leader sequence (1). According to recent studies, human RNase P is also required for transcription of tRNA, rRNA, and other small noncoding RNA genes by polymerase I and III (2, 3). RNase P activity is present in all domains of life (eukarya, archaea, and bacteria), as well as in subcellular organelles, mitochondria, and chloroplasts, with the exceptional case of the archaeon *Nanoarchaeum equitans* (4). In almost every organism, RNase P is a ribonucleoprotein complex consisting of one RNA subunit and of proteins that vary in number and size (from one in bacterial up to ten in human RNase P) (5, 6). Although both RNA and protein subunits are essential for activity *in vivo*, the RNase P RNA subunit from bacteria, some archaea, and human is catalytically active *in vitro* independently of proteins and in the presence of high ionic strength (7–9). There are two recently reported exceptions of RNase P lacking an RNA subunit; RNase P from human mitochondria and *Arabidopsis thaliana* mitochondria/chloroplasts are comprised of three protein subunits and only one protein subunit, respectively (10, 11).

The variety of the protein components and the necessity of the RNA subunit for catalysis raise questions on the molecular evolution of essential ribonucleoprotein complexes of the contemporary translational machinery. The protein content of RNase P is increased from bacteria to eukaryotes. The presence of each protein subunit in the eukaryal holoenzymes is necessary for the cell's viability (12). Noticeably, there is sequence homology

between some archaeal and some eukaryal RNase P protein subunits, but no homology was found with the bacterial proteins.

The human RNase P contains ten protein subunits (hPop5, hPop1, Rpp40, Rpp38, Rpp30, Rpp29, Rpp25, Rpp21, Rpp20, and Rpp14) (6), four of which reveal homology with the archaeal ones (Rpp30, hPop5, Rpp29, and Rpp21) (13–17). The yeast holoenzyme consists of nine proteins, homologues with human RNase P (hPop5/Pop5, hPop1/Pop1, Rpp30/Rpp1, Rpp29/Pop4, Rpp21/Rpr2, Rpp38/Pop3, Rpp20/Pop7, Rpp14/Pop8, and Rpp25/Pop6). Open reading frames, homologous to human protein counterparts, have been detected in a variety of eukaryotic and archaeal genomes (18).

Several studies have revealed the importance of specific protein–protein and RNA–protein interactions within the RNase P “core” complex for the formation of the catalytic core of 5' pre-tRNA processing activity. It is now established that four protein subunits are interacting primarily in pairs (Rpp30–Pop5 and Rpp29–Rpp21) and contact directly the RNA subunit, thus forming a minimum, enzymatically active core that in some cases can also be reconstituted *in vitro* (19). Crystal structures of the archaeal homologues of Rpp29 reveal the existence of exposed basic and hydrophobic residues on the protein's surface, indicating the ability of the protein to interact with other proteins and RNAs (20, 21). Both crystallographic and genetic analyses suggest the strong interaction between the Rpp29 and Rpp21 subunits from archaea, as well as from human (22–25). Recent studies demonstrate that Rpp29–Rpp21 heterodimer binds to and stabilizes the S-domain of the RNA subunit (19, 26, 27). Furthermore, Rpp29–Rpp21 complex causes a decrease on the ionic requirements for activity and improves the substrate binding affinity of the RNA. It must be noticed that in some cases Rpp29–Rpp21 together with the RNA form a minimum catalytic

*Corresponding authors. D.D.: tel, +30-61-997746; fax, +30-61-997690; e-mail, Drainas@med.upatras.gr. A.V.: e-mail, vourekas@mail.med.upenn.edu.

core (15, 28). Although archaeal and eukaryotic RNase P proteins have neither sequence nor structural similarity with C5 protein,¹ it has been reported that the human Rpp29 can substitute effectively the bacterial protein and form an active complex with M1 RNA *in vitro* (29).

RNase P from *Dictyostelium discoideum* has been previously characterized and displays the lowest buoyant density (1.23 g/mL) among the eukaryal RNase P holoenzymes studied so far (30), suggesting high protein content. Initial bioinformatic analysis indicated a protein complement with significant similarity to the human rather than the yeast enzymatic complex. DRpp30, DRpp40, and DRpp20 were verified as RNase P subunits in *D. discoideum* by biochemical and immunological approaches (31, 32). *D. discoideum* genome encodes five additional putative RNase P protein subunits (DRpp29, DRpp25, DRpp21, dPop5, and dPop1), often containing uncommon sequence features such as low complexity and *D. discoideum* specific domains (31, 32).

Rpp29 is an integral part of the minimum catalytic core of the archaeal and eukaryal RNase P holoenzymes, and that prompted us to characterize this protein in *D. discoideum*. Its gene was cloned, and antibodies were raised against the recombinant protein verified its participation in the RNase P RNP complex. Moreover, we provide biochemical evidence on the RNase P RNA subunit, which was previously characterized via comparative phylogenetic analysis (33). Based on the domain architecture of DRpp29, three DRpp29 deletion mutants were constructed in order to specify the domain that is responsible for the interaction with the RNA subunit. The structural elements of the RNA that contribute to the specific interaction with the DRpp29 protein subunit are also presented. Finally, DRpp29 and its mutants were tested in heterologous reconstitution experiments for their ability to form active RNase P complexes with M1 RNA. Kinetic analysis of these experiments revealed the characteristics of this intriguing functional complementation.

MATERIALS AND METHODS

RNase P Purification and Assay for RNase P Activity. Growth of *D. discoideum* cells (strain AX2 wild type), cell breakage, and the production of S-100 fraction were carried out as previously described (31). Enzyme assays were carried out at 37 °C in 20 μ L buffer D (50 mM Tris-HCl, pH 7.6, 5 mM MgCl₂, 10 mM NH₄Cl) in the presence of 5 fmol of labeled transcript of the *Schizosaccharomyces pombe* tRNA^{Ser} gene SupS1 and 1.3 μ g of protein from the RNase P fraction. The reactions were stopped by addition of 5 μ L of stop dye (80% formamide, 50 mM EDTA, 0.1% bromophenol blue, 0.1% xylene cyanol). Reaction products were resolved on 10% polyacrylamide/8 M urea gels. The purification procedure consisting of one step of anion-exchange chromatography (DE-52 cellulose) followed by cation-exchange chromatography (P-11 phosphocellulose) and another anion-exchange chromatography (DE-52 cellulose) as a final step was carried out as previously described (34). Throughout this work, a Phosphorimager Fuji-film FLA 3000 and AIDA software were used for visualization and quantification purposes of radioactive signals.

Northern Blotting. Partially purified RNase P was phenol extracted followed by ethanol precipitation for the isolation of RNA present in these fractions, hereafter named pRNA. One microgram of pRNA and 10 μ g of total RNA from *D. discoideum* at myxamoeba stage were analyzed by 6% 8 M urea polyacrylamide gel electrophoresis and electrotransferred (80 V, 4 h at 4 °C) onto Zeta-Probe membrane. The blot was hybridized with three probes: a 5' (5'-GAATATTACATTGGTTTCAAACCA-ATACC-3', positions 1–29), an internal (5'-TTTCCCAACC-TTTGTCATACTG-3', positions 247–268), and a 3' probe (5'-AGTATCAGTTAGAGATTAATCTGAATTGAG-3', positions 336–366). All probes were labeled on the 5' end using T4 polynucleotide kinase (Takara) and [γ -³²P]ATP. Hybridization was performed overnight at 50 °C in 0.5 M Na₂HPO₄, pH 7.2, 1 mM EDTA, and 7% SDS.

Primer Extension and 3' RACE of RNase P RNA. One microgram of pRNA was mixed with 0.1 pmol of 5' labeled primer 5'-TTTCCCAACCTTTGTCATACTG-3' in hybridization buffer (1.25 M KCl, 1 mM EDTA, 10 mM Tris, pH 7.9), heated at 80 °C for 10 min, and then cooled slowly to 30 °C. The RNA was reverse transcribed in the presence of 5 units of AMV RT (Finnzymes), 5 mM MgCl₂, 2.5 mM DTT, and 0.165 mM dNTPs at 47 °C for 45 min. For sequencing reactions, ddNTPs were present at a final concentration of 0.18 mM. The reaction mixtures were phenol extracted, and the cDNA products were precipitated by ethanol and analyzed by denaturing 6% PAGE.

RNA from partially purified RNase P was polyadenylated at the 3' end using poly(A) polymerase (Takara) in the presence of 10 mM MgCl₂, 2.5 mM MnCl₂, 250 mM NaCl, 250 μ M ATP, and 0.005% BSA at 37 °C for 15 min. Poly(A) RNase P RNA was reverse transcribed by AMV RT in the presence of a poly(T) anchor primer (5'-GACCACGCGTATCGATGTCGACTTT-TTTTTTTTTTTTTTTT-3'), and the cDNAs were amplified using forward primer 5'-GAGAATAATATGGGAAGGTCTGAG-3' (positions 87–110) and reverse anchor primer 5'-GACC-ACGCGTATCGATGTCGAC-3'. PCR fragments were directly cloned using the TOPO-TA method, and five clones were sequenced twice.

Cloning of the RNase P RNA Subunit. A set of primers was designed (sense, 5'-TAATACGACTCACTATAGGGTA-TTGGTTTGAACCA-3'; antisense, 5'-ACTAGTATCAGT-TAGAGATTAATCTG-3'), located exactly at the 5' and 3' ends of the gene, as these were determined by our experimental approach, the same as identified by Marquez and colleagues (33). Sense primer incorporates the T7 promoter (underlined) directly upstream the gene sequence, and antisense primer incorporates *Spe*I restriction site for the generation of runoff transcription template after cloning in the pUC19 vector. The sequence was amplified by PCR using *D. discoideum* (AX4) genomic DNA as template. The PCR conditions included an initial denaturation step at 95 °C for 2 min, 35 cycles of 94 °C for 30 s, 44 °C for 40 s, and 67 °C for 40 s, and a final extension step at 67 °C for 10 min. The transcript was synthesized by a T7 RNA polymerase reaction in which ribonucleotide molar ratios reflected the occurrence of each residue in the sequence of RNase P RNA.

Run-off transcription of the RNA subunit (both the mature and the F1 truncated fragment; see Results) was performed at 4 °C, 16 °C, 37 °C, and room temperature. The transcripts were preincubated at room temperature for 20 min in a 20 μ L reaction containing 50 mM Tris-HCl, pH 7.6, 100 mM NH₄Cl, and various concentrations of MgCl₂ ranging from 1 to 100 mM. The mixtures were incubated from 30 min to 24 h at 4 °C, 16 °C,

¹Abbreviations: M1 RNA, *Escherichia coli* RNase P RNA; C5 protein, *E. coli* RNase P protein; SDS-PAGE, sodium dodecyl sulfate-polyacrylamide gel electrophoresis; EDTA, ethylenediaminetetraacetic acid; RNP, ribonucleoprotein; pSupS1, precursor *Schizosaccharomyces pombe* suppressor tRNA^{Ser}; pRNA, precursor tRNA.

23 °C, 30 °C, 37 °C, and room temperature and assayed for activity.

Enzymatic Structure Analysis of the RNase P RNA and Footprinting Analysis of the RNase P RNA–DRpp29 Complex. For these experiments, *in vitro* transcribed RNase P RNA was labeled at the 5' end using T4 polynucleotide kinase and [γ - 32 P]ATP. The labeled RNA was purified using Sephadex G-25 quick spin columns (Roche, 11273990001), and final concentration was adjusted at 100 ng/ μ L. Ambion's RNase T1 and RNase A were used, with reagents and buffers supplied (Ambion AM2283). For generation of nucleotide "ladder", 3 μ L of 5' labeled RNase P RNA was mixed with 2 μ g (2 μ L) of yeast RNA and incubated with 10 μ L of alkaline buffer for 3 min. Reaction was stopped on ice and by adding 10 μ L of loading buffer (Ambion, AM8547). For the determination of T1 cleavage sites under denaturing conditions (3' end of all G residues), 1 μ L of 5' labeled RNase P RNA was mixed with 0.7 μ g (1 μ L) of yeast RNA, 2 μ L of H₂O, and 6 μ L of RNA sequencing buffer, incubated at 50 °C, cooled at room temperature, and treated with 0.1 unit of RNase T1 at room temperature. Reaction was stopped by adding 20 μ L of inactivation buffer. Reaction products were ethanol precipitated, washed with 70% EtOH, dried, dissolved in 7 μ L of gel loading buffer, incubated at 95 °C for 5 min, and left on ice until electrophoresis. For the determination of single-stranded Gs, Us, and Cs, 1 μ L of 5' labeled RNase P RNA was mixed with 0.7 μ g (one μ L) of yeast RNA, 6 μ L of H₂O, and 1 μ L of 10 \times RNA structure buffer, either 0.1 unit of RNase T1 or RNase A, and incubated at room temperature for 15 min. Reaction was stopped, precipitated, and prepared as above. Cleavage products were analyzed on a 6% denaturing polyacrylamide gel.

5' labeled RNase P RNA (0.3 pmol) was preincubated with various amounts of purified recombinant DRpp29 as described below for mobility shift assay, followed by RNase T1 treatment under native conditions for the determination of the protein binding sites on the RNA, as described above.

Cloning and Preparation of the Recombinant DRpp29 Protein and the Δ 75, Δ 155, and NTR Polypeptides. Based on the genomic DNA sequencing data available in dictyBase (<http://www.dictybase.org/>), the complete open reading frame of *drpp29* (759 bp) was amplified and cloned by RT-PCR using total RNA. Three truncated fragments were also cloned, δ 75, δ 155, and δ NTR, by PCR on the cloned *drpp29* gene. The primers used were *drpp29* (Fwd, 5'-ATGAAAAAATAATAAAAAAG-3'; Rev, 5'-TCATAATTCGATATTCTTACGAG-3'), δ 75 (Fwd, 5'-GAGAATATAGATAAACCATTTGTA-3'; Rev, 5'-TCA-TAATTCGATATTCTTACGAG-3'), δ 155 (Fwd, 5'-CCCGC-TCTTGTAATAAAA-3'; Rev, 5'-TCATAATTCGATATTCT-TACGAG-3'), and δ NTR (Fwd, 5'-ATGAAAAAATAATAAAAAAG-3'; Rev, 5'-TCACATCAACTATATCTTTCC-3').

All of the genes were cloned into the pET29c expression vector (Novagen) bearing a C-terminal His₆ tag. The *Escherichia coli* BL21(DE3)-Rosetta and -Codon Plus competent cells were transformed with these constructs. An adequate quantity of all of the recombinant polypeptides was detected in the soluble protein fraction, from which the polypeptides were affinity purified on a Ni²⁺-nitriloacetic acid agarose column (Qiagen). SDS-PAGE analysis and Coomassie staining of the gels determined the high purity of the recombinant polypeptides. The purified polypeptides were dialyzed in a buffer containing 200 mM NaCl, 100 mM NaH₂PO₄, 10 mM Tris-HCl, pH 7.6, and 25% glycerol.

Production of Rabbit Polyclonal Antibodies and Immunoprecipitation Assays. Two rabbits were immunized by four chronically separated subcutaneous injections with 100 μ g of the purified recombinant DRpp29. Sera collected the 52nd day after the first immunization injection were the most enriched in anti-DRpp29 antibodies, as determined by ELISA.

The assays were essentially performed as described previously (31). Briefly, pre- or postimmune sera coated protein A Sepharose beads were incubated with partially purified RNase P preparations overnight at 4 °C in buffer D (50 mM Tris-HCl, pH 7.6, 10 mM NH₄Cl, 5 mM MgCl₂, 0.1 unit/ μ L RNasin). The beads were washed three times with IPP150 (10 mM Tris-HCl, pH 8.0, 0.1% Nonidet P-40, 0.5 mM PMSF, 150 mM NaCl) and three times with buffer D. Both pellets and supernatants were assayed for RNase P activity.

Mobility Shift Assay. [γ - 32 P]ATP labeled transcript of RNase P RNA (0.35 pmol) was incubated with purified recombinant polypeptides DRpp29, Δ 75, Δ 155, and NTR for 20 min at 30 °C. The 20 μ L reaction was carried out in 1 \times binding buffer (10 mM Tris-HCl at pH 8, 100 mM KCl, 5 mM MgCl₂, 1 mM DTT, 1 mM EDTA, and 10% glycerol) in the presence or absence of unlabeled RNase P RNA or total yeast RNA. The unlabeled RNAs were preincubated with the polypeptides for 10 min at 30 °C before the addition of labeled molecules. All of the RNA molecules were heat denatured at 90 °C for 1 min and renatured on ice for 2 min. The RNA-protein complexes were analyzed by electrophoresis on a 4% native polyacrylamide gel in 1 \times TB buffer (35 mM Tris-base, 17.5 mM boric acid), containing 1 mM MgCl₂ and 5% glycerol, at 4 °C.

Kinetic Analysis of the Heterologous RNase P Complexes. Three picomoles of M1 RNA and 30 pmol of purified DRpp29 or Δ 75 were preincubated for 3 h at 37 °C in 20 μ L reaction buffer (50 mM Tris-HCl at pH 7.6, 10 mM MgCl₂, 100 mM NH₄Cl). Reaction rates were measured from the slopes of the time plots in the presence of labeled (1 nM) and various concentrations of unlabeled SupS1 at 37 °C. Bacterial RNase P activity was reconstituted by mixing 0.1 pmol of M1 RNA and 0.5 pmol of C5 protein in the same buffer as above for 30 min at 37 °C. One picomole of M1 ribozyme was preincubated in 20 μ L of reaction buffer (50 mM Tris-HCl at pH 7.6, 50 mM MgCl₂, 100 mM NH₄Cl) for 30 min at 37 °C. Reaction rates were measured from the slopes of the time plots in the presence of labeled (1 nM) and various concentrations of unlabeled SupS1 at 37 °C. For each kinetic curve, at least three independent experiments were performed.

Modeling and Prediction of Potential RNA Binding Residues in DRpp29. The three-dimensional structure of the 137–252 region of DRpp29 (DRpp29_{137–252}) was constructed through comparative modeling by using MODELER v9.1 (35) based on the recently solved crystal structure of *Pyrococcus horikoshii* PhoRpp29 RNase P protein (PDB ID: 2ZAE) (24). Electrostatic potential maps were calculated with MOLMOL (36).

RESULTS

Characterization of RNase P RNA Subunit. The putative *D. discoideum* RNase P RNA subunit gene was identified by Marquez and colleagues (33) through phylogenetic comparative analysis. We detected the transcript of this gene by RT-PCR in total RNA and RNA extracted from partially purified RNase P preparations (data not shown). Interestingly, Northern analysis of the same samples using a probe that hybridizes at positions 247–268 of the predicted RNase P RNA gene (Figure 1A)

yielded three signals: a predominant band (marked “M”) which corresponds to the size of the predicted gene transcript (369 nts), a band with a smaller size (~300 nts) (marked “F1”), and a band migrating slower than the mature transcript (marked with an asterisk), possibly representing a precursor form of the mature transcript. This slower migrating band was present only in total RNA fractions but not in RNase P preparations (Figure 1A, left panel, lane 3 versus lanes 4 and 5). Next, the same samples were probed using oligos hybridizing at the 5' and 3' ends of the RNase P RNA transcript. This analysis indicated that band M harbors the predicted 5' and 3' ends as it is recognized by both probes (Figure 1A, middle and right panels). On the contrary, band F1 is recognized by 3' probe but not 5' probe, and it is obviously a 5' truncated form of the RNase P RNA which harbors an intact 3' end.

To determine the exact 5' and 3' termini of the observed RNase P RNA fragments, we performed primer extension and 3' RACE analysis using RNA extracted from partially purified, native RNase P. Primer extension analysis (Figure 1B) showed that there are two predominant termination points of reverse transcriptase mediated cDNA synthesis (marked with arrows), one that corresponds to the predicted 5' end of the mature RNA subunit (G1) and a second one (A75), which is most likely the 5' end of the truncated form (F1 fragment) that was also uncovered by Northern analysis. Moreover, 3' RACE analysis determined one major 3' terminus, C369 (data not shown), implying that both the mature RNase P RNA and the F1 fragment share a common 3' end. We have no substantial information on the biogenesis and possible functional role of the F1 RNA fragment, and we cannot exclude the possibility that it represents a random degradation product. However, its occurrence in total RNA preparations and in active RNase P preparations has been consistent.

Concerning the secondary structure of *D. discoideum* RNase P RNA, there are two previous relevant reports. Piccinelli et al. (37) reported a prediction of the P3 structural element based on phylogenetic analysis, and a second study by Zhu et al. (38) reported the prediction of the overall fold of the RNA subunit by the MFold algorithm. The two presented structures exhibit differences, and neither is supported by experimental data. Thus, we probed the secondary structure of the *in vitro* transcript of the RNase P RNA by nuclease footprinting analysis, and we incorporated the experimental data in a proposed fold that also satisfies phylogenetic restrictions.

We treated RNase P RNA with ribonucleases T1 and A under native conditions (Figure 1C, lanes 3 and 4, respectively), and we compared with T1 treatment under denaturing conditions (Figure 1C, lane 1) to identify G, C, and U residues that remain single stranded or paired in double-stranded structural elements. This treatment produced a specific and reproducible pattern, suggesting that the *in vitro* transcript adopts a specific fold dictated by its primary sequence. Restrictions from previous phylogenetic analysis of RNase P RNA structure (33, 37) and the results of enzymatic footprinting were incorporated in the model of the secondary structure presented in Figure 1D. *D. discoideum* RNase P RNA harbors all conserved features of eukaryotic RNase P RNA (CR I–V; P1, P2, P3, P4; a four-way junction consisting of eP5/7, P8, P9, P10/11; and P12) and also an extended P3 helix divided in P3a and P3b by an internal bulge loop (L3), an extended S domain with characteristic elements such as P10.1 and P11, and a P19 helix harboring a 15-residue A-rich loop (L19). A P15 element, which is present in some eukaryotes like *Saccharomyces cerevisiae*, is absent.

We have previously reported that after extensive deproteinization of the ribonucleoprotein complex of *D. discoideum* RNase P a new endonucleolytic activity was revealed that was attributed to the RNase P RNA (39). We assayed the *in vitro* transcript of the RNase P RNA gene in a wide variety of conditions, in short and prolonged incubations, but we were unable to determine a robust nucleolytic RNase P activity.

Cloning, Sequence Analysis, and Modeling of DRpp29. Based on the annotated sequence of *D. discoideum drpp29* (*D. dictyostelium* cDNA database, www.dictybase.org), a pair of primers was designed, and the *drpp29* ORF was cloned using RT-PCR on total RNA. The cloned ORF and the annotated sequence were identical.

The *drpp29* ORF (759 bps) encodes a positively charged protein (pI 9.6) consisting of 252 amino acid residues, with a molecular mass of 29.317 kDa. A multiple sequence alignment among DRpp29 and several eukaryotic (*Homo sapiens*, *Mus musculus*, *Drosophila melanogaster*, *S. cerevisiae*, and *S. pombe*) and archaeal (*P. horikoshii* and *Methanocaldococcus jannaschii*) homologues (Figure 2A) reveals a universal C-terminal domain, whereas DRpp29 and its eukaryotic homologues contain extended N-termini, absent from archaeal orthologues (Figure 2B). Although there is a significant degree of similarity in these eukaryotic specific domains, the N-terminus appears to be unique for each protein or similar only in closely related sequences (for example, human and mouse sequences have similar N-termini, Figure 2A). This region in DRpp29 comprises the first 75 amino acid residues and was designated as NTR (N-terminal region) (Figure 2B). On the basis of this analysis we cloned and over-expressed in bacteria wild-type DRpp29 and three truncation mutants: $\Delta 75$ which lacks the NTR and could be considered as the minimal eukaryotic core, $\Delta 155$ which corresponds to the p29 core that is present in all p29 proteins, and NTR alone (Figure 2B).

Modeling of DRpp29 was limited to the 137–252 region (DRpp29_{137–252}) on the basis of available sequence homology with known structures (19, 24). The structural model of DRpp29_{137–252} consists of a six-stranded antiparallel β -sheet ($\beta 1$ to $\beta 6$) and five helices (Figure 3). The β -barrel core of DRpp29_{137–252} folds into a Sm-like fold. The majority of the residues implicated in protein–protein interactions in *Pyrococcus furiosus* PfuRpp29 (19) and *P. horikoshii* PhoRpp29 (24) are also conserved in DRpp29 (Figure 3A). The opposite region that is consisted of $\beta 1$, $\beta 2$, $\beta 5$, $\beta 6$, $\alpha 3$, and $\alpha 4$ could be occupied for RNA interactions. Moreover, a NMR chemical shift perturbation mapping upon titration of *Methanothermobacter thermoautotrophicus* Rpp29 (Mth Rpp29) with the Mth RNA subunit revealed several residues likely important in RNA binding (40) (Figure 3E). These residues are conserved in DRpp29 (Figure 3E) and are located opposite to the surface of the protein that could be implicated in protein–protein interaction. The electrostatic potential map of DRpp29 identified surface patches with positive electrostatic potential on different faces of the complex (Figure 3B,D). The largest of these positively charged surfaces spans the face of the protein that is not implicated in protein interactions (Figure 3D). Several highly conserved Arg and Lys residues are located in this surface patch. K161 is located in helix $\alpha 3$, K176 in $\beta 1$, K178 in a loop structure between $\beta 1$ and $\beta 2$, K186 in the strand $\beta 2$, K202 in the loop between $\beta 3$ and $\beta 4$, K205 in $\beta 4$, and K230 in helix $\alpha 4$, and K242, K243, R247, and K248 are located in the C-terminus of the β -barrel core of DRpp29_{137–252}.

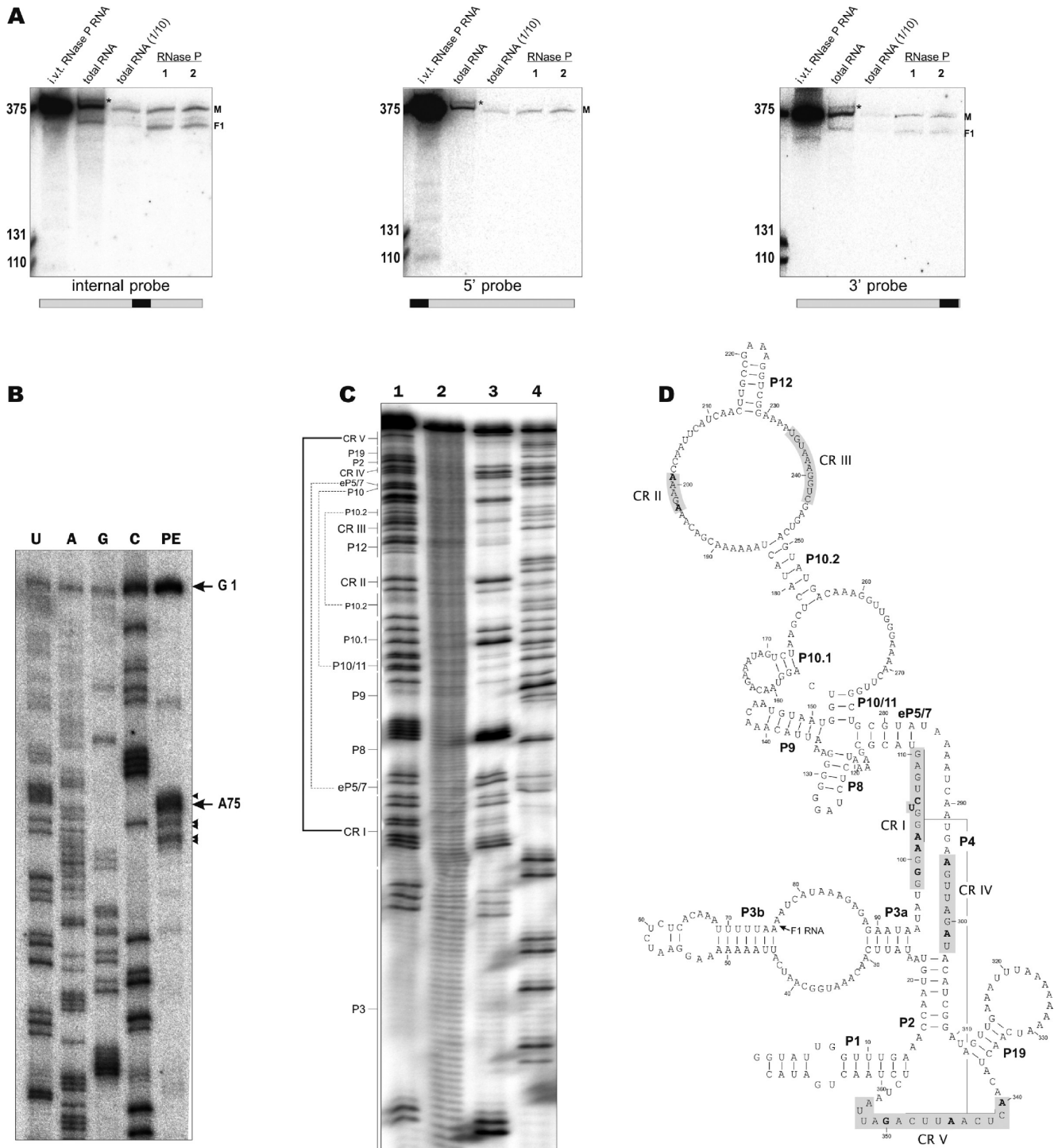


FIGURE 1: Characterization of *D. discoideum* RNase P RNA. (A) Northern blot analysis of *D. discoideum* total RNA and RNase P samples using probes hybridizing on various positions on the RNase P RNA transcript. On the left margin of each blot the sizes of three labeled RNA markers are indicated. Left panel: Hybridization with an internal probe (position 247–268). Middle panel: Hybridization with 5' probe (position 1–29). Right panel: Hybridization with 3' probe (position 336–366). At the bottom of each blot, the relative position of each probe (black box) on the RNase P RNA transcript (gray) is indicated graphically. Possible precursor RNase P RNA transcript and mature RNase P RNA are recognized by all three probes and are marked with an asterisk and with M, respectively, 5' truncated form is recognized by internal and 3' probe and is marked F1. (B) Primer extension analysis of native RNase P RNA. RNA extracted from RNase P active fractions was extended with reverse transcriptase (lane PE). The sequencing ladder reactions were generated in the presence of ddNTPs (lanes U, A, G, C). Bands representing the 5' ends of the two predominant RNA species are marked with arrows G1 and A75 (lane PE) and correspond to mature RNA and F1 RNA, respectively (arrowheads indicate less frequent 5' ends and/or reverse transcriptase termination by strong secondary structure). (C) Enzymatic structure analysis of the *in vitro* transcribed RNase P RNA. The 5' labeled transcript was subjected to partial enzymatic or chemical cleavage for determination of its secondary structure. Lane 1: RNase T1 cleavage products of RNase P RNA under denaturing conditions (cleavage after G residues). Lane 2: Alkaline hydrolysis of RNA. Lane 3: RNase T1 cleavage products of RNase P RNA under native conditions (cleavage after single-stranded G residues). Lane 4: RNase A cleavage products of RNase P RNA (cleavage after single-stranded C and U residues). On the left, secondary structure elements are marked; dashed lines connect paired strands, bold lines connect conserved regions CR I and CR II, which form a P4 pseudoknot. (D) Secondary structure of RNase P RNA. Universally conserved residues are in bold, conserved regions are marked CR I–V and shaded gray, and helical elements are numbered P1–19. The 5' end of the F1 RNase P RNA fragment is marked on J3b/3a with an arrow.

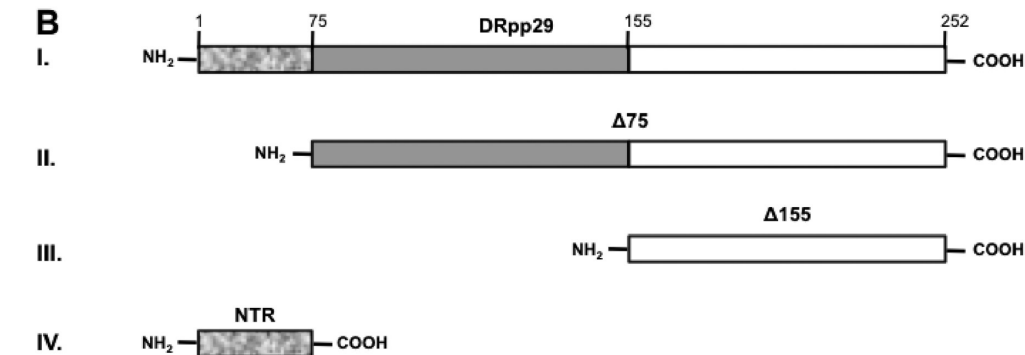
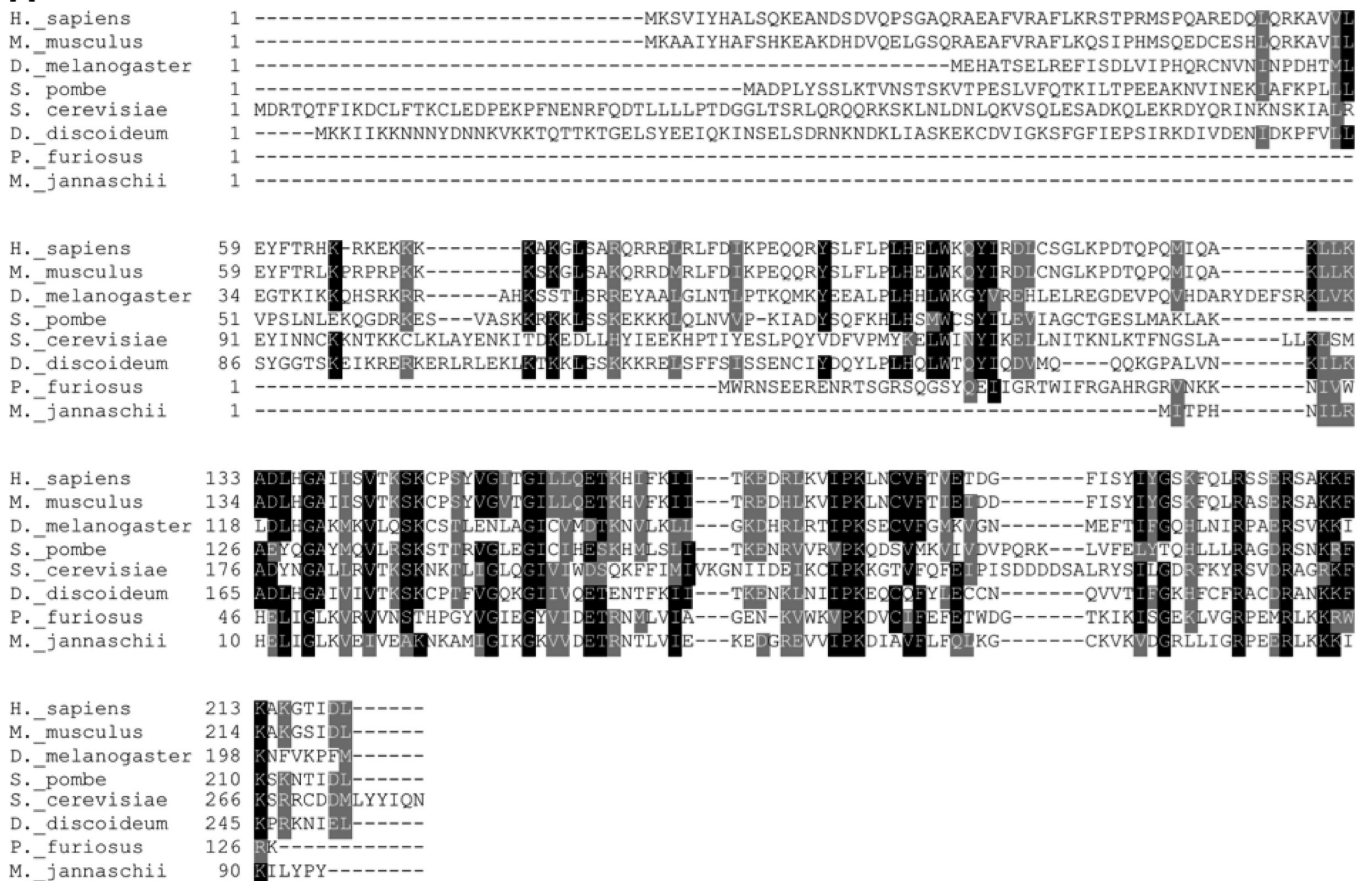
A

FIGURE 2: (A) Multiple sequence alignment (ClustalW (56)) of DRpp29 (HM_452383) with eukaryotic and archaeal potential homologues (*H. sapiens*, NP_006404; *M. musculus*, NC_000073.5; *D. melanogaster*, NP_648168; *S. cerevisiae*, NP_011929; *S. pombe*, XP_001713139; *P. furiosus*, NP_579545; *M. jannaschii*, NP_247439). The residues exhibiting identity and similarity are highlighted in black and gray, respectively, with a 60% threshold using BLOSUM scoring matrix. (B) Graphical representation of the three structural features of DRpp29 based on the level of similarity with its counterparts. (I) DRpp29 protein (the numbers above the scheme correspond to the amino acids). (II) The minimal eukaryal DRpp29 which lacks the *D. discoideum* specific NTR (mutant $\Delta 75$). (III) The carboxy-terminal core region, which is present in all p29 proteins (mutant $\Delta 155$). (IV) The amino-terminal sequence specific for *D. discoideum* (mutant NTR).

DRpp29 Is a Subunit of the *D. discoideum* RNase P Complex. To confirm the participation of DRpp29 in the RNase P holoenzyme complex, the recombinant DRpp29-His₆ was purified after overexpression of the corresponding gene in *E. coli* and used in its native form for immunization of rabbits. Pre- and postimmune serum was used for Western blot analysis of samples collected during the last purification step of RNase P (Figure 4A). Anti-DRpp29 polyclonal antibodies recognize a band, which coincides with RNase P activity obtained after the third purification step on the DE-52 column (Figure 4B). These polyclonal antibodies were tested for pulling down RNase P activity by immunoprecipitation. Pre- and postimmune sera were

bound to protein A Sepharose beads and incubated with partially purified RNase P. The beads were washed under stringent conditions to ensure the specificity of the DRpp29 and anti-DRpp29 antibody interaction. While preimmune serum failed, postimmune serum coated beads efficiently immunoprecipitated RNase P activity (Figure 5, compare lane 4 (preimmune) with lane 6 (postimmune)). We also observed significant RNase P depletion from the supernatant (85%) (Figure 5, compare lane 3 (preimmune) with lane 5 (postimmune)).

DRpp29 Binds to RNase P RNA: An N-Terminal Region Is Required for the Binding. For catalysis, the *D. discoideum* RNase P RNA functions in cooperation with

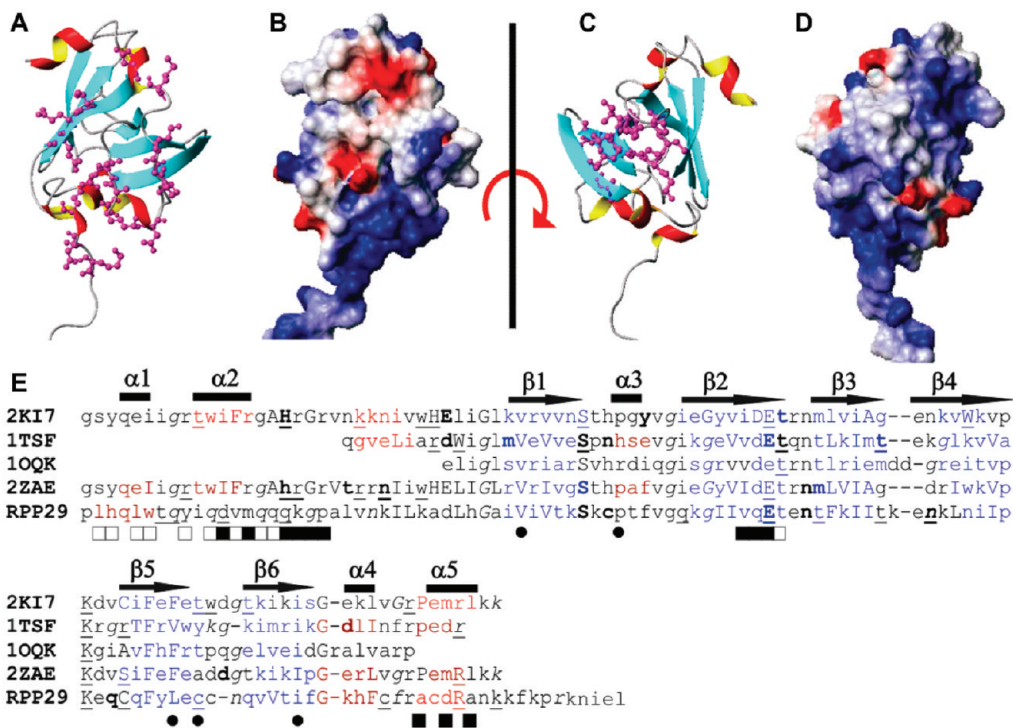


FIGURE 3: Structural model of the DRpp29 protein subunit of the *D. discoideum* RNase P holoenzyme. In (A) is shown the surface of the protein that is implicated in protein–protein interactions (DRpp21), whereas in (C) the opposite surface is illustrated. Residues that are implicated in protein–protein interactions and protein–RNA interactions are colored in magenta in (A) and (C), respectively. In (B) [the orientation is the same as in (A)] and (D) [the orientation is the same as in (C)] the electrostatic surface potential of DRpp29 is displayed as a color gradient from red (negative) to blue (positive). (E) Structure-based sequence alignment of DRpp29 with high-resolution structures of other homologues: Rpp29 from *P. furiosus* (PDB ID: 2KI7) (25), aRpp29 from *Archaeoglobus fulgidus* (PDB ID: 1TSF) (21), MthRpp29 from *M. thermoautotrophicus* (PDB ID: 1OQK) (40), and PhoRpp29 from *P. horikoshii* (PDB ID: 2ZAE) (24). The sequence alignment is in JOY format (57) that contains information about secondary structures, solvent accessibility, and hydrogen bonding. Specifically, residues that are solvent inaccessible are in upper case, solvent accessible are in lower case, located in α helix are colored in red, located in beta strand are colored in blue, located in 3-10 helix are colored in maroon, implicated in hydrogen bond to main chain amide are in bold, implicated in hydrogen bond to main chain carbonyl are underlined, and have positive ϕ angles are in italics. The symbols ■, □, and ● denote residues that have been implicated in protein–protein interactions with Rpp21 (hydrogen bonds and salt bridges), the interface residues, and RNA–protein interactions, respectively. The information concerning the interface residues in protein–protein interactions has been extracted from PDB IDs 2KI7 and 2ZAE of the NMR and X-ray structures of Rpp29–Rpp21 complexes by PISA (http://www.ebi.ac.uk/msd-srv/prot_int/pistart.html). The information on the implication of residues in RNA interactions came from the literature (40). Furthermore, electrostatic potential analysis suggests a possible RNA-binding surface of DRpp29.

protein subunits. It is therefore essential to understand which individual protein subunit, in the context of the holoenzyme, and how it facilitates the appropriate conformation for catalytic activity. Although a comprehensive understanding of the mechanism of *D. discoideum* RNase P would necessitate elaborate studies of all subunits and their interactions, mechanistic details of the holoenzyme function could be revealed through the characterization of DRpp29 and its interaction with the catalytic RNase P RNA. Indeed, earlier studies have shown that both human and yeast Rpp29 function via direct interaction with their respective RNase P RNA subunit (22, 41, 42). In order to probe the potential of direct interaction of DRpp29 with the *D. discoideum* RNase P RNA, electrophoretic mobility shift assays were performed. As illustrated in Figure 6A, DRpp29 forms a specific complex with the RNA subunit (white arrow, lanes 2–4), in agreement with previous reports from human, yeast, and archaea (41–43). The stoichiometry of the complex is one DRpp29 per one RNA subunit, and the dissociation constant (K_D) is 8 nM. The stoichiometry was calculated by electrophoretic mobility shift assays with decreasing concentration of RNA and simultaneously increasing concentration of DRpp29, as has been previously described by Ambrogelly et al. (44). Moreover, the dissociation constant (K_D) was calculated from the slopes of

the Scatchard plots obtained from electrophoretic mobility shift assays (data not shown). The formation of DRpp29/RNase P RNA complexes is inhibited very efficiently by unlabeled RNase P RNA (Figure 6, lanes 5–7), whereas addition of an excess of total yeast RNA used here as a nonspecific competitor had only a minor effect (lanes 5–7 versus lane 8). These competition experiments support the specificity of the interaction between DRpp29 and RNase P RNA. In a similar experiment, DRpp29 could not interact with labeled pSupS1, which is routinely used as a substrate of eukaryal RNase P (data not shown).

We next tested which of the truncation mutants that were designed retains the RNA binding specificity. $\Delta 75$ (amino acids 76–252) and $\Delta 155$ (amino acids 156–252) correspond to a minimal eukaryal and archaeal p29, respectively, while NTR (amino acids 1–75) corresponds to the N-terminal *D. discoideum* specific domain (Figure 2B). $\Delta 75$ forms a stable and specific complex with the RNA subunit, with a stoichiometry 1:1, and the dissociation constant (K_D) is 3.9 nM. The stoichiometry and the dissociation constant are estimated, as described above for the formation of the DRpp29–RNA complex. The $\Delta 75$ /RNase P RNA complex is very sensitive to the addition of unlabeled RNase P RNA as a specific competitor, while it tolerates up to about 28 times the amount of a nonspecific competitor compared

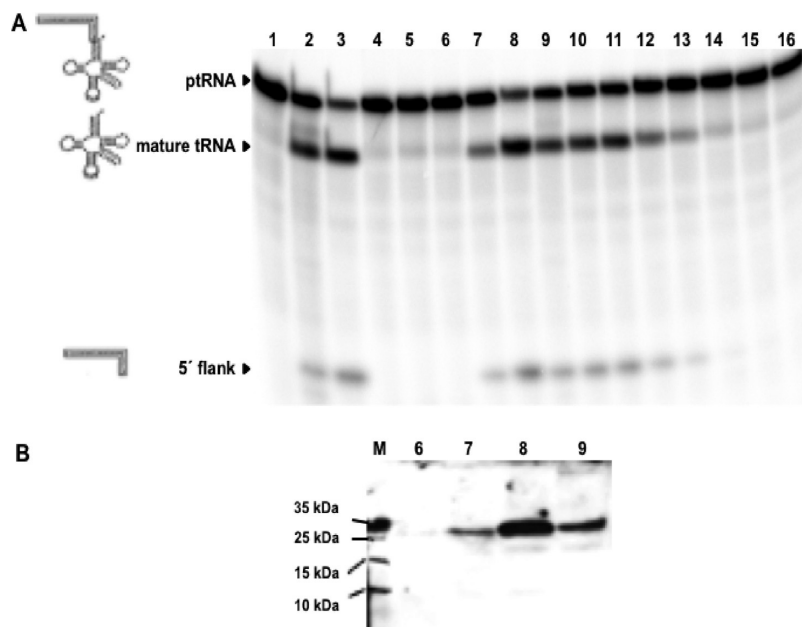


FIGURE 4: DRpp29 copurifies with *D. discoideum* RNase P activity. (A) Fractions from the final purification step were assayed for RNase P activity using ^{32}P -labeled pSupS1 as substrate. Reaction products were electrophoretically analyzed on a 10% polyacrylamide/8 M urea gel. Lanes: 1, pSupS1 alone; 2, control RNase P reaction; 3, flow-through sample; 4, wash sample; 5–16, eluted fractions from DE-52 column. RNase P cleaves the pSupS1 (110 nucleotides), producing the mature tRNA (82 nucleotides) and the 5' leader sequence (5' flank, 28 nucleotides). The corresponding bands are marked on the left margin. (B) The same fractions were subjected to Western blot analysis using anti-DRpp29. DRpp29 was detected only in the catalytically active *D. discoideum* RNase P fractions. The positions of the protein molecular mass markers are also indicated.

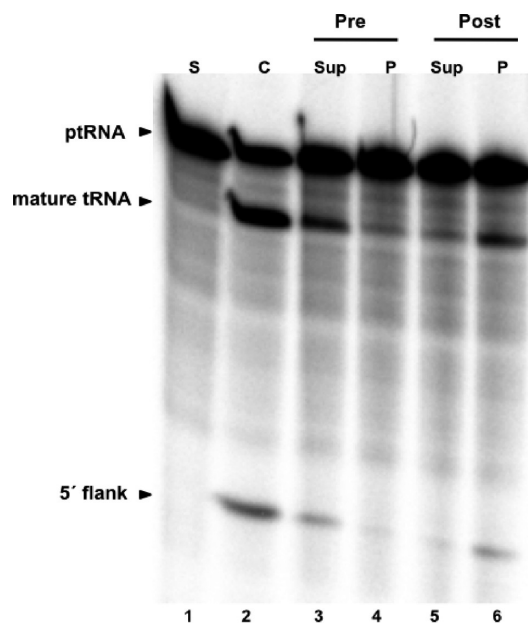


FIGURE 5: Immunoprecipitation of RNase P activity using polyclonal antibodies against DRpp29. Pre- (lanes 3 and 4) or postimmune rabbit antiserum (lanes 5 and 6) was used to immunoprecipitate RNase P activity from a partially purified *D. discoideum* RNase P preparation. The supernatants (lanes 3 and 5) and the pellets (lanes 4 and 6) were assayed for RNase P activity. Lane 1: pSupS1 alone (S). Lane 2: control RNase P reaction (C).

to the specific one (Figure 6B, compare lanes 11 and 14). Surprisingly, $\Delta 155$ did not bind the RNA subunit in our assay, and neither did NTR. This result was largely unexpected: $\Delta 155$ comprises the required residues to fold into the archaeal Sm-fold (p29 core) as shown by our modeling analysis, which in turn carries the necessary elements to bind its cognate RNase P RNA

in the context of the archaeal RNP complex. We noticed a series of lysine and arginine residues forming a potentially conserved, low complexity region within the eukaryotic specific N-terminus of DRpp29, which is present in $\Delta 75$ but not in $\Delta 155$. This region spans positions 92–118, and out of the 27 residues, 10 are lysines and 5 are arginines (Figure 2A). It is possible that this Lys/Arg-rich region facilitates the interaction of DRpp29 with the RNA subunit and helps the conserved p29 core to dock on the RNA more efficiently. It is important to note here that NTR is also rich in lysines, especially at the first 18 residues, 7 of which are lysines. However, NTR did not show a similar RNA binding activity, even when it was added in great excess in the assay mixture (Figure 6B). This observation suggests that our assay is not indiscriminately detecting all possible interactions between positively charged peptides with RNA, which supports the specificity of the results described above.

Finally, to identify the regions of the RNA that interact with DRpp29, we performed enzymatic footprinting analysis. During DRpp29–RNase P RNA interaction, we observed that nucleotides G114 and G116 located in eP5/7, G127 and G128 located in the P8 stem, and the G158 located in the P10.1 stem are the residues that exhibit the most prominent protection from T1 RNase degradation in the presence of DRpp29 (Figure 7).

DRpp29 and M1 RNA Reconstitute a Heterologous RNase P Complex. On the basis that human protein Rpp29 and M1 RNA can form an active RNase P complex (29, 45), it was tested whether DRpp29 can also activate M1 RNA at low magnesium concentration (10 mM $[\text{Mg}^{2+}]$) (7). Noticeably, the DRpp29–M1 RNA complex could efficiently remove the 5' leader sequence from the SupS1 substrate, and the activity of the heterologous complex peaked at a DRpp29:M1 RNA molar ratio of 20:1 (Figure 8, lane 7). The recombinant DRpp29 preparations used were not contaminated with C5 protein, as confirmed by Western blot analysis using affinity-purified polyclonal

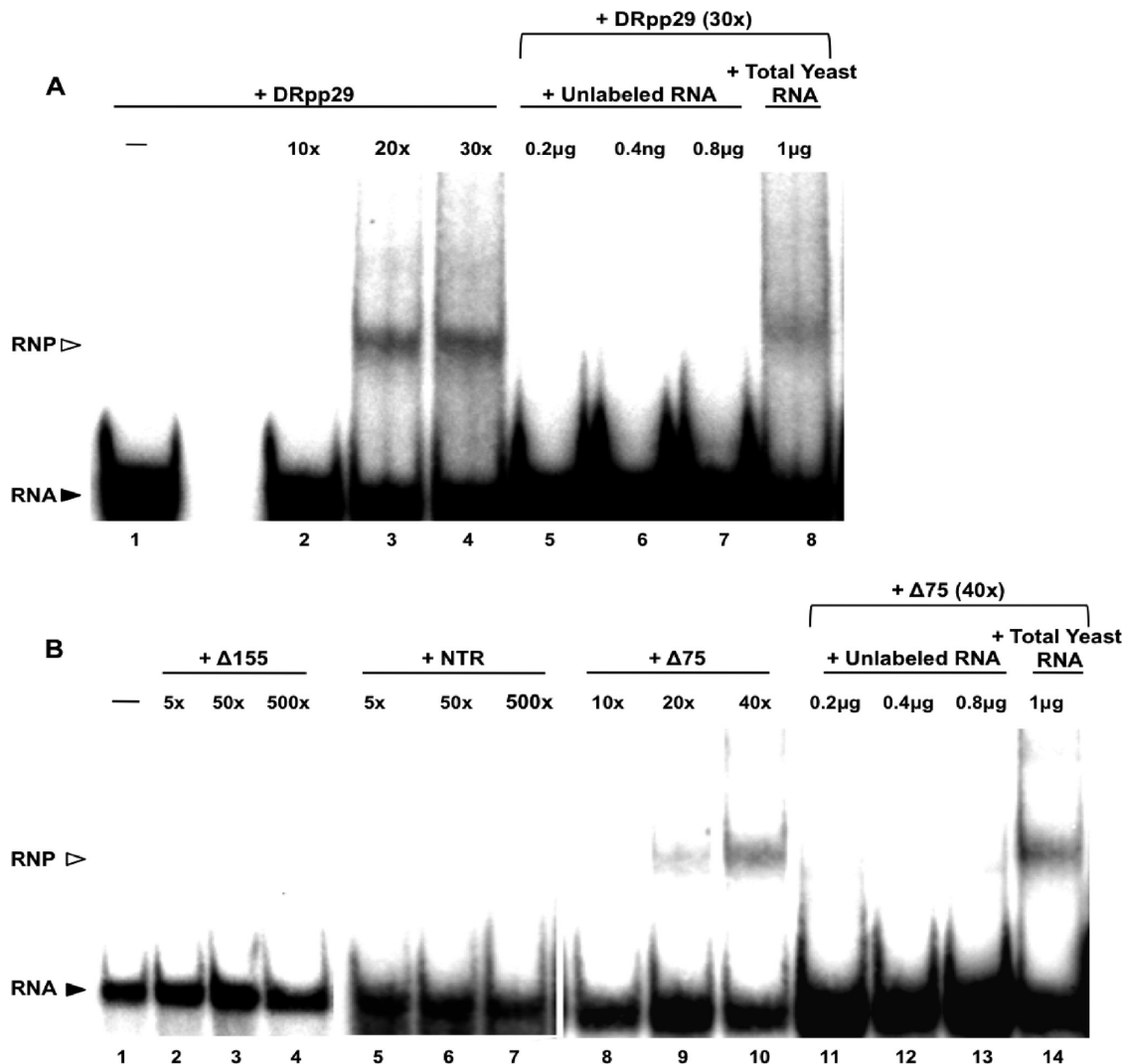


FIGURE 6: Electrophoretic mobility shift assay of the *D. discoideum* RNase P RNA. (A) Gel shift of the *D. discoideum* RNase P RNA in the presence of DRpp29. Internally ^{32}P -labeled RNase P RNA (0.35 pmol) (lane 1) was incubated in the presence of increasing amounts of DRpp29 (lanes 2–4). The formation of the ribonucleoprotein complex was inhibited by the presence of increasing concentrations of unlabeled RNase P RNA (lanes 5–7). Total yeast RNA (lane 8) did not affect the formation of the complex. (B) Gel shift of the RNase P RNA subunit in the presence of the polypeptides $\Delta 155$, NTR, and $\Delta 75$. Lane 1: Internally ^{32}P -labeled RNase P RNA (0.35 pmol). Lanes 2–4: RNase P RNA in the presence of increasing amounts of $\Delta 155$. Lanes 5–7: RNase P RNA in the presence of increasing amounts of NTR. Lanes 8–10: RNase P RNA in the presence of increasing amounts of $\Delta 75$. The formation of the RNA– $\Delta 75$ complex was inhibited by the presence of increasing concentrations of unlabeled RNA (lanes 11–13) but was modestly affected by total RNA from yeast (lane 14). The positions of the free RNA and the DRpp29–RNA complex (RNP) are marked by a black and a white arrow, respectively, on the left margin.

anti-C5 antibodies (data not shown). The DRpp29 mutants NTR, $\Delta 75$, and $\Delta 155$ were used in similar reconstitution experiments with M1 RNA, and only $\Delta 75$, that contains the DRpp29_{95–118} Lys/Arg-rich region, could activate M1 RNA (Figure 8, lanes 9–11).

The kinetic constants of the reaction for the heterologous holoenzymes DRpp29–M1 RNA and $\Delta 75$ –M1 RNA were determined and were compared with those for the C5–M1 RNA holoenzyme and M1 ribozyme. The initial velocity was calculated by the initial slope of the time plots. The kinetic constants (K_m , V_{max}) of the four activities were calculated from the Michaelis–Menten diagrams by using the curve-fitting program Kaleidagraph (Figure 9). DRpp29 decreases the K_m value of the M1 RNA alone reaction, and the $\Delta 75$ polypeptide does not improve the K_m of M1, but its presence lowers the Mg^{2+} requirements of the ribozyme (Table 1). The estimated k_{cat} values indicate that DRpp29–M1 RNA, as well as $\Delta 75$ –M1 RNA, catalyzes the maturation of SupS1 substrate with a slower rate

than the C5–M1 RNA enzyme (Table 1). Noticeably, the V_{max} of the homologous C5–M1 RNA complex for the pSupS1 substrate compares well with those reported by Mann et al. (45).

DISCUSSION

Characterization of the RNase P RNA Gene. The experimental verification of the *D. discoideum* RNase P RNA subunit has provided interesting information. Apart from the mature size RNase P RNA transcript (370 nt), a larger transcript and 5' truncated form of the RNase P RNA gene were detected. The transcript with an apparent size of ~390 nucleotides was recognized by all three RNase P RNA probes used and most likely represents a precursor form of the mature transcript. Interestingly, this larger transcript was detected only in total RNA samples and not in RNA extracted from RNase P preparations. Söderbom and colleagues have identified a highly conserved sequence motif ([A/T]CCCA[C/T]AA) which lies approximately 63 nt upstream of the transcriptional start site

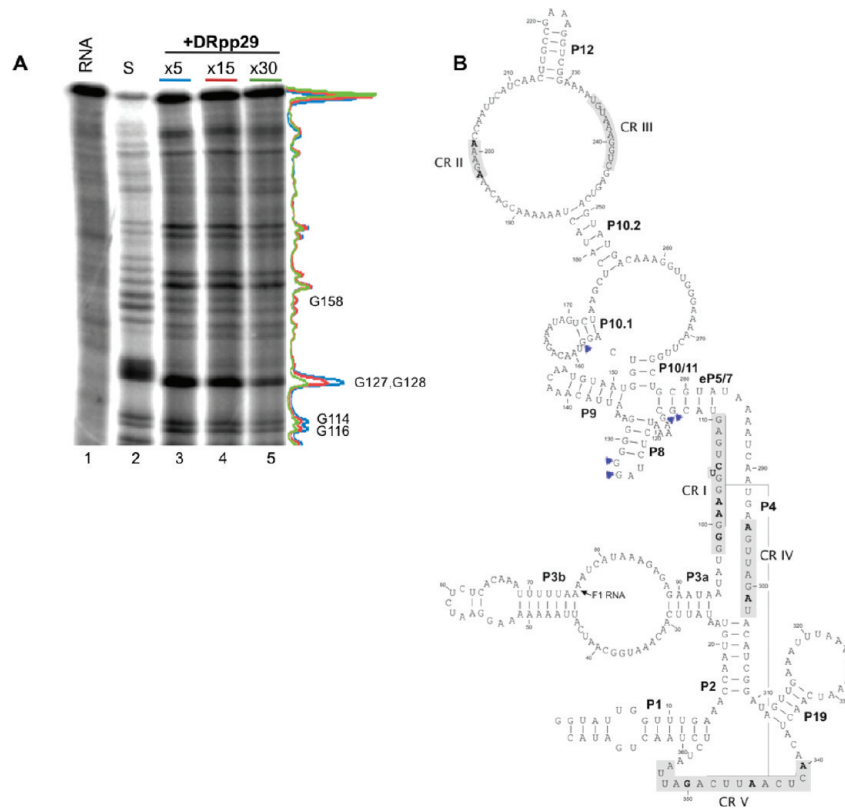


FIGURE 7: RNase T1 footprinting analysis of *D. discoideum* RNase P RNA in the presence of DRpp29. (A) The RNA subunit has been incubated with T1 ribonuclease in the absence or in the presence of DRpp29. Lane 1: [γ - 32 P]RNA alone. Lane 2: Denatured RNA treated with T1 ribonuclease. Lanes 3–5: Native form of RNA subunit treated with T1 in the presence of increasing amounts of DRpp29. The G residues protected by the presence of DRpp29 are indicated on the right of the autoradiograph. The band intensity was quantified by the AIDA software (colored lines). (B) *D. discoideum* RNase P RNA secondary structure. The arrows indicate the G nucleotides bound by DRpp29.

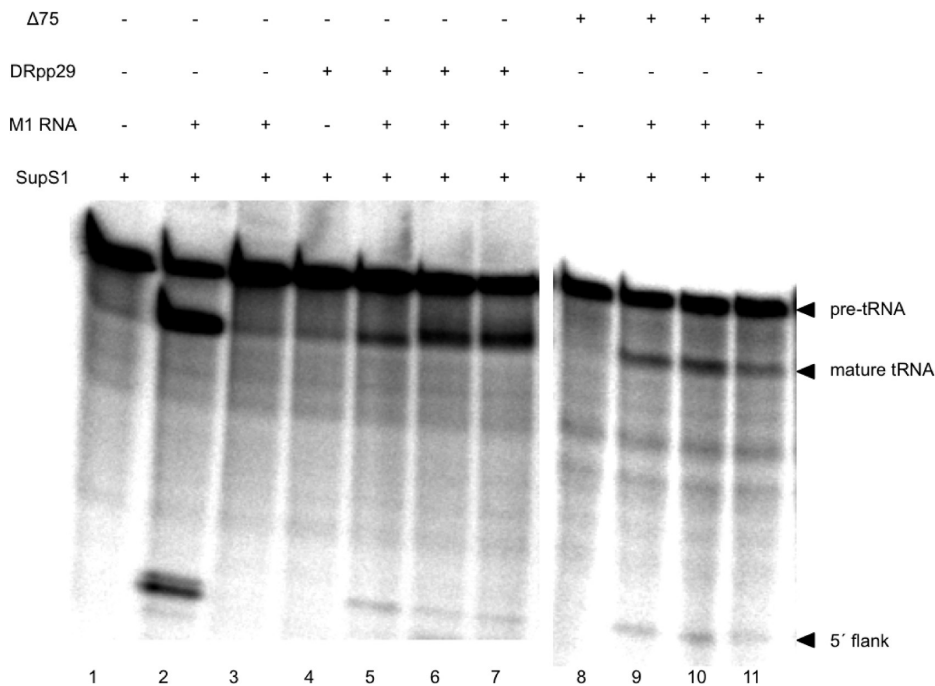


FIGURE 8: Autoradiograph of the cleavage of pSupS1 by the heterologous reconstituted complexes DRpp29–M1 RNA and $\Delta 75$ –M1 RNA. Lane 1: pSupS1 alone. Lane 2: RNase P control reaction. Lane 3: M1 RNA alone in the presence of 10 mM Mg^{2+} . Lane 4: DRpp29 alone. Lanes 5–7: M1 RNA in the presence of increasing amounts of DRpp29 (5 \times , 10 \times , and 20 \times , respectively) at 10 mM Mg^{2+} . Lane 8: $\Delta 75$ alone. Lanes 9–11: M1 RNA in the presence of increasing amounts of $\Delta 75$ (5 \times , 10 \times , and 20 \times , respectively) at 10 mM Mg^{2+} .

of *D. discoideum* noncoding RNA genes (46, 47). This element (TCCATAA) is present 88 nts upstream of the 5' end of RNase P RNA, thus suggesting the production of a precursor RNase P

RNA of about 390 nt, which is in accordance with the size of the observed large transcript in the Northern blot experiments (Figure 1). If this is indeed a precursor form of RNase P RNA, it

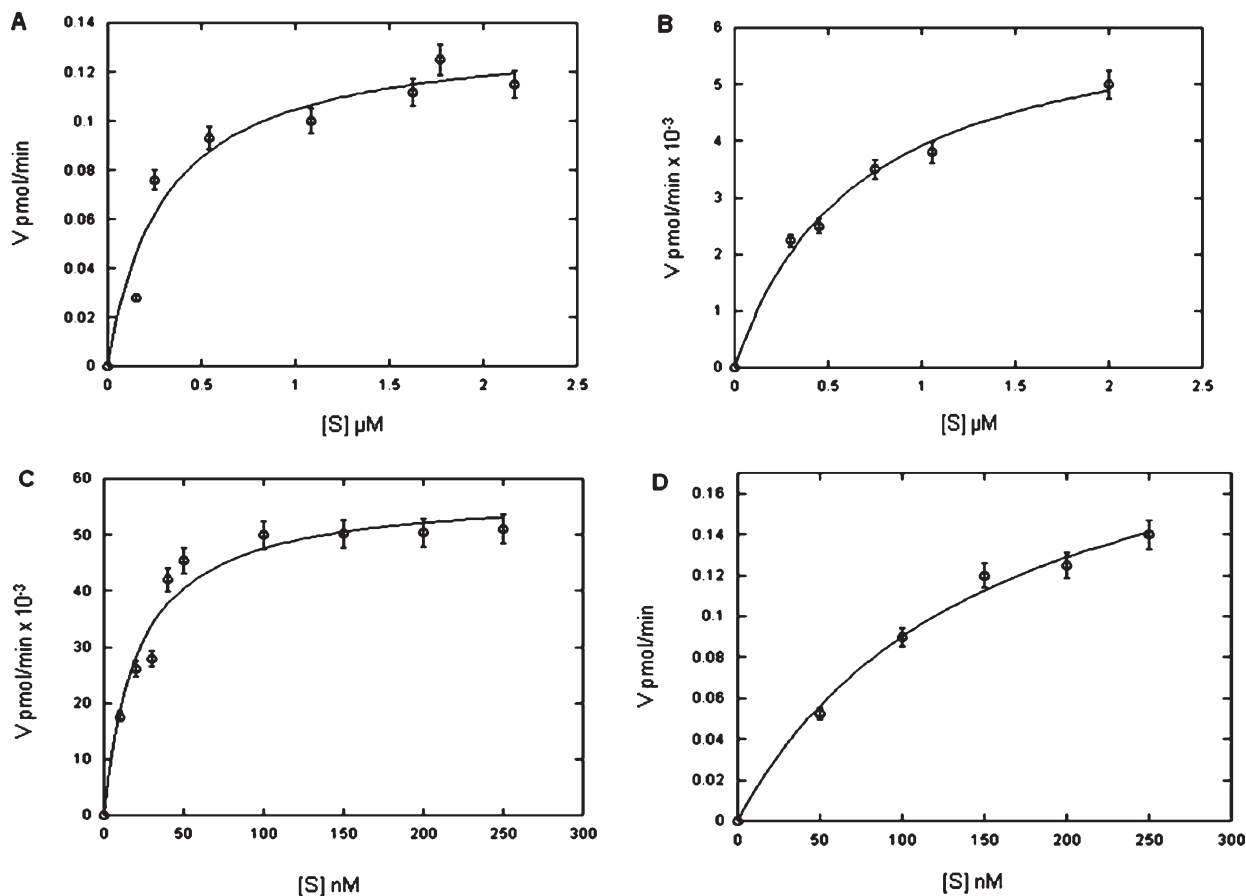


FIGURE 9: Kinetic analysis of the RNase P reconstituted activities for pSupS1 substrate. Michaelis–Menten diagrams of (A) the M1 RNA–DRpp29 complex, (B) the M1 RNA– $\Delta 75$ complex, (C) the M1 RNA–C5 complex, and (D) the M1 RNA alone.

Table 1: Estimated Kinetic Parameters K_m , V_{max} , and k_{cat} and Ratio k_{cat}/K_m of the Reconstituted Complexes and the M1 RNA Alone^a

	K_m (nM)	V_{max} (pmol/min)	k_{cat} (min^{-1})	k_{cat}/K_m ($\text{min}^{-1} \mu\text{M}^{-1}$)
M1 RNA–C5 (10 mM Mg^{2+})	151 ± 0.27	0.232 ± 0.02	2.2	14.57
M1 RNA (50 mM Mg^{2+})	471 ± 0.06	0.205 ± 0.01	0.41	0.87
M1 RNA–DRpp29 (10 mM Mg^{2+})	299 ± 0.1	0.135 ± 0.01	0.045	0.15
M1 RNA– $\Delta 75$ (10 mM Mg^{2+})	662 ± 0.06	$6.5 \times 10^{-3} \pm 0.01$	2.2×10^{-3}	3.32×10^{-3}

^aThe standard errors of the curve fits shown in Figure 8 are indicated in the estimates of K_m and V_{max} .

will be very interesting to identify the process that gives rise to the mature product.

Concerning the 5' truncated fragment of RNase P RNA, we have no information on its possible biogenesis. This fragment appears both in total RNA and in RNase P preparations and follows ion exchange eluted RNase P activity (data not shown) that is free of contaminating exonucleases, an observation confirmed by Northern blot and primer extension analyses (Figure 1A,B, absence of smaller fragments). Moreover, the full-length RNase P RNA/F1 RNA ratio does not change even after prolonged storage of the enzymatic preparations. Although we cannot exclude the possibility that this is an artifact generated during lysate preparation, the above observations make it less likely that the F1 RNA fragment is a random degradation product of the RNase P RNA transcript. Moreover, despite the fact that the function of F1 RNA is not yet known, this is not the first time that two RNA species have been detected in active RNase P fractions. Specifically, nuclear RNase P from the fission yeast *S. pombe* copurifies with two RNA species, K1 and K2 (48). Based on the proposed RNase P RNA secondary structure, F1

RNA fragment lacks an intact P3 element. The importance and underlying biology of these observations are currently under examination.

Secondary structure analysis by enzymatic footprinting supports an elementary eukaryotic fold, with an extended P3 element, a four-way junction consisting of eP5/7, P8, P9, and P10/11, an extended S domain harboring a rather uncommon configuration of P10, P10.1, and P11 elements, the ancestral P12 element (49), and a P19 helix. We acknowledge that the use of the *in vitro* transcript of RNase P RNA and only two different nucleases to report on its secondary conformation in these assays poses a limit to the extent that these results can be interpreted. Nevertheless, treated RNA yielded a reproducible pattern, and conserved elements such as P3, pseudoknot P4, the four-way junction, and P12 were accurately identified, suggesting that our approach is pertinent and provides valid information.

The description of the secondary structure of the *D. discoideum* RNase P RNA may provide information on the mode of action of small molecule effectors, such as protein synthesis inhibitors and retinoids, which have been reported to exhibit strong

inhibitory effect on eukaryotic RNase P activity (50–52). As already mentioned, efforts for identifying a ribonucleolytic activity of the RNase P RNA transcript *in vitro* that can be reliably characterized were unsuccessful. Although elusive so far, such an activity cannot be excluded, and there is an ongoing effort in our laboratory to determine optimal assay conditions that would allow its reliable detection.

Characterization of DRpp29 Protein. In the present report we describe the features of the recombinant DRpp29 protein subunit of *D. discoideum* RNase P. DRpp29 is a positively charged protein, which aligns well with homologues from eukaryotic and archaeal RNase P holoenzymes (20, 53). Three distinct domains can be identified within DRpp29 by sequence similarity (Figure 2B, starting from the C-terminus): the common in archaea and eukarya p29 core, a eukaryotic specific domain harboring a Lys/Arg-rich region, and a N-terminal region that displays relatively low conservation. Polyclonal antibodies, produced against DRpp29, confirmed its participation in the RNase P RNP complex.

In order to correlate the functional and structural features of DRpp29, structural modeling was performed. Based on the sequence homology of the protein with the available protein structures, DRpp29_{137–252} was modeled and found to adopt an Sm-like fold. In the electrostatic potential map of the β -barrel core of the protein, patches with electropositive potential could be located. Furthermore, several areas that potentially mediate protein–protein and protein–RNA interactions were identified and provide the basis for future functional–mutational studies (Figure 3).

The analysis of the RNase P RNA binding potential of DRpp29 was a logical goal for our study, as this is a common feature of p29 proteins in both archaeal and eukaryotic RNase P. Indeed, DRpp29 binds efficiently *Dictyostelium* RNase P RNA *in vitro*. Moreover, it was found that the p29 core domain of DRpp29 (mutant Δ 155) was unable to form stable complexes with the RNA subunit, despite having all necessary structural elements for proper folding. Intriguingly, a truncation mutant representing a presumed minimal eukaryotic p29 sequence (Δ 75) was particularly efficient in binding RNase P RNA (Figure 6). The Δ 75/RNase P RNA complex can resist very large amounts of a nonspecific competitor, but it is sharply inhibited by small amounts of a specific competitor. A Lys/Arg-rich region at the N terminus of Δ 75 appears to be conserved in eukaryotes (Figure 2A), and we propose that this region facilitates the formation of this protein–RNA complex. Nevertheless, we cannot assume that the p29 core is not essential for this interaction, and most likely, it is still required for proper recognition and positioning of eukaryotic p29 proteins onto RNase P RNA. Our results suggest that the eukaryotic p29–RNase P RNA interface has developed different characteristics that set it apart from the archaeal counterpart.

Footprinting analysis of the RNase P RNA in the presence of DRpp29 showed that the sites of DRpp29 binding on the RNase P RNA (Figure 7) most probably lie on the elements eP5/7, P8, and P10.1. P8 and P10.1 are located in the specificity domain of the RNA subunit (S-domain), and eP5/7 connects the C- (catalytic) domain with the S-domain. DRpp29 binding to the S-domain is in agreement with previous report, suggesting that the binary complex Rpp29–Rpp21 stabilizes the recognition of different substrates by human RNase P (45). Consistent with this observation, studies demonstrate that Rpp29–Rpp21 heterodimer binds to and stabilizes the S-domain of the RNA

subunit (19, 26, 27, 54, 55). Similarly, it was shown that *Pfu* Rpp29–Rpp21 does not alter the k_{cat} of the *Pfu* RNase P RNA catalyzed reaction while it decreases the K_m 5-fold and lowers the Mg^{2+} requirement (15). Additionally, reconstitution experiments with archaeal type M RNase P RNA (*M. jannaschii*) tethered with pre-tRNA substrate suggest that Rpp29–Rpp21 improves substrate affinity by binding to the S-domain (28).

DRpp29 and M1 RNA Reconstitute an Active RNase P Complex. Despite the fact that the human homologue Rpp29 could form an active complex with the M1 RNA (29), up to now no sequence or structural similarity had been reported between Rpp29 proteins and C5 protein. In the current study, it was found that DRpp29 could form a catalytic complex with M1 RNA under low Mg^{2+} concentration, as in the case of human Rpp29 (45) (Figure 8, lanes 5–7). The role of DRpp29 to promote this RNA-based catalysis seems to be assigned on elements located in its N-terminal domain, since it was identified that among its deletion mutants that were constructed only the Δ 75 construct could form an active complex with M1 RNA (Figure 8, lanes 9–11). The way that DRpp29 can replace C5 and induces M1 RNA folding in its catalytic active state would require the determination of the three-dimensional structure of this complex. Since footprints of C5 and DRpp29 on the *E. coli* RNase P RNA are different, it seems that the mechanism of action of these two proteins is likely to be distinct. Sharin and colleagues (29) have reported that the C-terminal domain of human Rpp29 is responsible for M1 RNA activation, and this has been attributed mainly to the conserved Lys162 and His163 residues (“KH motif”). This motif is absent from DRpp29 (Figure 2A), and a negatively charged residue (Glu194) is located in the relevant position of Lys162 of the “KH motif” of human Rpp29. In a very recent study it was found that *P. horikoshii* RNase P protein *PhoRpp29*, although it presented sequence homology to the C-terminal two-thirds of Rpp29, could not activate M1 RNA (26). These observations indicate a potential functional differentiation between *PhoRpp29* and Rpp29. Interestingly, the sequence of *PhoRpp29* lacks the conserved sequence pattern located both in DRpp29 and in Rpp29, and this could explain this discrepancy.

ACKNOWLEDGMENT

We thank Dr. Constantinos Stathopoulos for discussion and critical reading of the manuscript. The plasmids pDW98/M1RNA and pQE30/C5 were generous gifts of Dr. Roland Hartmann. The antibody anti-C5 was the generous gift of Dr. Agustín Vioque.

REFERENCES

1. Vourekas, A., Stamatopoulou, V., Toumpeki, C., Tsilaidou, M., and Drinas, D. (2008) Insights into functional modulation of catalytic RNA activity. *IUBMB Life* 60, 669–683.
2. Reiner, R., Krasnov-Yoeli, N., Dehtiar, Y., and Jarrous, N. (2008) Function and assembly of a chromatin-associated RNase P that is required for efficient transcription by RNA polymerase I. *PLoS One* 3, e4072.
3. Jarrous, N., and Reiner, R. (2007) Human RNase P: a tRNA-processing enzyme and transcription factor. *Nucleic Acids Res.* 35, 3519–3524.
4. Randau, L., Schroder, I., and Soll, D. (2008) Life without RNase P. *Nature* 453, 120–123.
5. Hall, T. A., and Brown, J. W. (2002) Archaeal RNase P has multiple protein subunits homologous to eukaryotic nuclear RNase P proteins. *RNA* 8, 296–306.
6. Jarrous, N. (2002) Human ribonuclease P: subunits, function, and intranuclear localization. *RNA* 8, 1–7.

7. Guerrier-Takada, C., Gardiner, K., Marsh, T., Pace, N., and Altman, S. (1983) The RNA moiety of ribonuclease P is the catalytic subunit of the enzyme. *Cell* 35, 849–857.
8. Pannucci, J. A., Haas, E. S., Hall, T. A., Harris, J. K., and Brown, J. W. (1999) RNase P RNAs from some Archaea are catalytically active. *Proc. Natl. Acad. Sci. U.S.A.* 96, 7803–7808.
9. Kikovska, E., Svard, S. G., and Kirsebom, L. A. (2007) Eukaryotic RNase P RNA mediates cleavage in the absence of protein. *Proc. Natl. Acad. Sci. U.S.A.* 104, 2062–2067.
10. Holzmann, J., Frank, P., Löffler, E., Bennett, K. L., Gerner, C., and Rossmannith, W. (2008) RNase P without RNA: identification and functional reconstitution of the human mitochondrial tRNA processing enzyme. *Cell* 135, 462–474.
11. Gobert, A., Gutmann, B., Taschner, A., Gössringer, M., Holzmann, J., Hartmann, R. K., Rossmannith, W., and Giegé, P. (2010) A single *Arabidopsis* organellar protein has RNase P activity. *Nat. Struct. Mol. Biol.* (Epub ahead of print).
12. Chamberlain, J. R., Lee, Y., Lane, W. S., and Engelke, D. R. (1998) Purification and characterization of the nuclear RNase P holoenzyme complex reveals extensive subunit overlap with RNase MRP. *Genes Dev.* 12, 1678–1690.
13. Kakuta, Y., Ishimatsu, I., Numata, T., Kimura, K., Yao, M., Tanaka, I., and Kimura, M. (2005) Crystal structure of a ribonuclease P protein Ph1601p from *Pyrococcus horikoshii* OT3: an archaeal homologue of human nuclear ribonuclease P protein Rpp21. *Biochemistry* 44, 12086–12093.
14. Terada, A., Honda, T., Fukuhara, H., Hada, K., and Kimura, M. (2006) Characterization of the archaeal ribonuclease P proteins from *Pyrococcus horikoshii* OT3. *J. Biochem.* 140, 293–298.
15. Tsai, H. Y., Pulukkunat, D. K., Woznick, W. K., and Gopalan, V. (2006) Functional reconstitution and characterization of *Pyrococcus furiosus* RNase P. *Proc. Natl. Acad. Sci. U.S.A.* 103, 16147–16152.
16. Kawano, S., Nakashima, T., Kakuta, Y., Tanaka, I., and Kimura, M. (2006) Crystal structure of protein Ph1481p in complex with protein Ph1877p of archaeal RNase P from *Pyrococcus horikoshii* OT3: implication of dimer formation of the holoenzyme. *J. Mol. Biol.* 357, 583–591.
17. Wilson, R. C., Bohlen, C. J., Foster, M. P., and Bell, C. E. (2006) Structure of Pfu Pop5, an archaeal RNase P protein. *Proc. Natl. Acad. Sci. U.S.A.* 103, 873–878.
18. Hartmann, E., and Hartmann, R. K. (2003) The enigma of ribonuclease P evolution. *Trends Genet.* 19, 561–569.
19. Xu, Y., Amero, C. D., Pulukkunat, D. K., Gopalan, V., and Foster, M. P. (2009) Solution structure of an archaeal RNase P binary protein complex: formation of the 30-kDa complex between *Pyrococcus furiosus* Rpp21 and Rpp29 is accompanied by coupled protein folding and highlights critical features for protein-protein and protein-RNA interactions. *J. Mol. Biol.* 393, 1043–1055.
20. Numata, T., Ishimatsu, I., Kakuta, Y., Tanaka, I., and Kimura, M. (2004) Crystal structure of archaeal ribonuclease P protein Ph1771p from *Pyrococcus horikoshii* OT3: an archaeal homolog of eukaryotic ribonuclease P protein Rpp29. *RNA* 10, 1423–1432.
21. Sidote, D. J., Heideker, J., and Hoffman, D. W. (2004) Crystal structure of archaeal ribonuclease P protein aRpp29 from *Archaeoglobus fulgidus*. *Biochemistry* 43, 14128–14138.
22. Jiang, T., and Altman, S. (2001) Protein-protein interactions with subunits of human nuclear RNase P. *Proc. Natl. Acad. Sci. U.S.A.* 98, 920–925.
23. Hall, T. A., and Brown, J. W. (2004) Interactions between RNase P protein subunits in archaea. *Archaea* 1, 247–254.
24. Honda, T., Kakuta, Y., Kimura, K., Saho, J., and Kimura, M. (2008) Structure of an archaeal homolog of the human protein complex Rpp21-Rpp29 that is a key core component for the assembly of active ribonuclease P. *J. Mol. Biol.* 384, 652–662.
25. Amero, C. D., Boomershine, W. P., Xu, Y., and Foster, M. (2008) Solution structure of *Pyrococcus furiosus* Rpp21, a component of the archaeal RNase P holoenzyme, and interactions with its Rpp29 protein partner. *Biochemistry* 47, 11704–11710.
26. Honda, T., Hara, T., Nan, J., Zhang, X., and Kimura, M. (2010) Archaeal homologs of human RNase P protein pairs Pop5 with Rpp30 and Rpp21 with Rpp29 work on distinct functional domains of the RNA subunit. *Biosci., Biotechnol., Biochem.* 74, 266–273.
27. Kosaka, S., Hada, K., Nakashima, T., and Kimura, M. (2010) Structural changes in ribonuclease P RNA in the hyperthermophilic archaeon *Pyrococcus horikoshii* OT3 induced on interaction with proteins. *Biosci., Biotechnol., Biochem.* 74, 394–396.
28. Pulukkunat, D. K., and Gopalan, V. (2008) Studies on *Methanocaldococcus jannaschii* RNase P reveal insights into the roles of RNA and protein cofactors in RNase P catalysis. *Nucleic Acids Res.* 36, 4172–4180.
29. Sharin, E., Schein, A., Mann, H., Ben-Asouli, Y., and Jarrous, N. (2005) RNase P: role of distinct protein cofactors in tRNA substrate recognition and RNA-based catalysis. *Nucleic Acids Res.* 33, 5120–5131.
30. Stathopoulos, C., Kalpaxis, D. L., and Drinas, D. (1995) Partial purification and characterization of RNase P from *Dictyostelium discoideum*. *Eur. J. Biochem.* 228, 976–980.
31. Vourekas, A., Kalavrizioti, D., Zarkadis, I. K., Spyroulias, G. A., Stathopoulos, C., and Drinas, D. (2007) A 40.7 kDa Rpp30/Rpp1 homologue is a protein subunit of *Dictyostelium discoideum* RNase P holoenzyme. *Biochimie* 89, 301–310.
32. Kalavrizioti, D., Vourekas, A., and Drinas, D. (2007) DRpp20 and DRpp40: Two protein subunits involved in *Dictyostelium discoideum* ribonuclease P holoenzyme assembly. *Gene* 400, 52–59.
33. Marquez, S. M., Harris, J. K., Kelley, S. T., Brown, J. W., Dawson, S. C., Roberts, E. C., and Pace, N. R. (2005) Structural implications of novel diversity in eucaryal RNase P RNA. *RNA* 11, 739–751.
34. Tekos, A., Stathopoulos, C., and Drinas, D. (1998) Bimodal action of alkaline earth cations on *Dictyostelium discoideum* ribonuclease P activity. *Biochemistry* 37, 15474–15480.
35. Sali, A., Potterton, L., Yuan, F., van Vlijmen, H., and Karplus, M. (1995) Evaluation of comparative protein modeling by MODELLER. *Proteins* 23, 318–326.
36. Koradi, R., Billeter, M., and Wüthrich, K. (1996) MOLMOL: a program for display and analysis of macromolecular structures. *J. Mol. Graphics* 14, 51–55.
37. Piccinelli, P., Rosenblad, M. A., and Samuelsson, T. (2005) Identification and analysis of ribonuclease P and MRP RNA in a broad range of eukaryotes. *Nucleic Acids Res.* 33, 4485–4495.
38. Zhu, Y., Stribinskis, V., Ramos, K. S., and Li, Y. (2006) Sequence analysis of RNase MRP RNA reveals its origination from eukaryotic RNase P RNA. *RNA* 12, 699–706.
39. Stathopoulos, C., Tekos, A., Zarkadis, I. K., and Drinas, D. (2001) Extensive deproteinization of *Dictyostelium discoideum* RNase P reveals a new catalytic activity. *Eur. J. Biochem.* 268, 2134–2140.
40. Boomershine, W. P., McElroy, C. A., Tsai, H. Y., Wilson, R. C., Gopalan, V., and Foster, M. P. (2003) Structure of Mth11/Mth Rpp29, an essential protein subunit of archaeal and eukaryotic RNase P. *Proc. Natl. Acad. Sci. U.S.A.* 100, 15398–15403.
41. Jiang, T., Guerrier-Takada, C., and Altman, S. (2001) Protein-RNA interactions in the subunits of human nuclear RNase P. *RNA* 7, 937–941.
42. Houser-Scott, F., Xiao, S., Millikin, C. E., Zengel, J. M., Lindahl, L., and Engelke, D. R. (2002) Interactions among the protein and RNA subunits of *Saccharomyces cerevisiae* nuclear RNase P. *Proc. Natl. Acad. Sci. U.S.A.* 99, 2684–2689.
43. Kouzuma, Y., Mizoguchi, M., Takagi, H., Fukuhara, H., Tsukamoto, M., Numata, T., and Kimura, M. (2003) Reconstitution of archaeal ribonuclease P from RNA and four protein components. *Biochem. Biophys. Res. Commun.* 306, 666–673.
44. Ambrogelly, A., Kamtekar, S., Stathopoulos, C., Kennedy, D., and Soll, D. (2005) Asymmetric behavior of archaeal propyl-tRNA synthetase. *FEBS Lett.* 579, 6017–6022.
45. Mann, H., Ben-Asouli, Y., Schein, A., Moussa, S., and Jarrous, N. (2003) Eukaryotic RNase P: role of RNA and protein subunits of a primordial catalytic ribonucleoprotein in RNA-based catalysis. *Mol. Cell* 12, 925–935.
46. Aspegren, A., Hinas, A., Larsson, P., Larsson, A., and Söderbom, F. (2004) Novel non-coding RNAs in *Dictyostelium discoideum* and their expression during development. *Nucleic Acids Res.* 32, 4646–4656.
47. Hinas, A., and Söderbom, F. (2007) Treasure hunt in an amoeba: non-coding RNAs in *Dictyostelium discoideum*. *Curr. Genet.* 51, 141–159.
48. Cherayil, B., Krupp, G., Schuchert, P., Char, S., and Söll, D. (1987) The RNA components of *Schizosaccharomyces pombe* RNase P are essential for cell viability. *Gene* 60, 157–161.
49. Sun, F. J., and Caetano-Anollés, G. (2010) The ancient history of the structure of ribonuclease P and the early origins of Archaea. *BMC Bioinf.* 11, 153–173.
50. Tekos, A., Tsagla, A., Stathopoulos, C., and Drinas, D. (2000) Inhibition of eukaryotic ribonuclease P activity by aminoglycosides: kinetic studies. *FEBS Lett.* 485, 71–75.
51. Tekos, A., Stathopoulos, C., Tsambaos, D., and Drinas, D. (2004) RNase P: a promising molecular target for the development of new drugs. *Curr. Med. Chem.* 11, 2979–2989.
52. Vourekas, A., Kalavrizioti, D., Stathopoulos, C., and Drinas, D. (2006) Modulation of catalytic RNA biological activity by small molecule effectors. *Mini Rev. Med. Chem.* 6, 971–978.

53. Jarrous, N., Eder, P. S., Wesolowski, D., and Altman, S. (1999) Rpp14 and Rpp29, two protein subunits of human ribonuclease P. *RNA* 5, 153–157.
54. Chen, W. Y., Pulukkunat, D. K., Cho, I. M., Tsai, H. Y., and Gopalan, V. (2010) Dissecting functional cooperation among protein subunits in archaeal RNase P, a catalytic ribonucleoprotein complex, *Nucleic Acids Res.* (Epub ahead of print).
55. Sinapah, S., Wu, S., Chen, Y., Pettersson, B. M. F., Gopalan, V., and Kirsebom, L. A. (2010) Cleavage of model substrates by archaeal RNase P: role of protein cofactors in cleavage-site selection, *Nucleic Acids Res.* (Epub ahead of print).
56. Thompson, J. D., Higgins, D. G., and Gibson, T. J. (1994) CLUSTAL W: improving the sensitivity of progressive multiple sequence alignment through sequence weighting, position-specific gap penalties and weight matrix choice. *Nucleic Acids Res.* 22, 4673–4680.
57. Mizuguchi, K., Deane, C. M., Blundell, T. L., Johnson, M. S., and Overington, J. P. (1998) JOY: protein sequence-structure representation and analysis. *Bioinformatics* 14, 617–623.